Bioorg. Med. Chem. 41 (2021) 116222

Contents lists available at ScienceDirect

Bioorganic & Medicinal Chemistry

journal homepage: www.elsevier.com/locate/bmc

Novel 1,3,4-oxadiazole compounds inhibit the tyrosinase and melanin level: Synthesis, *in-vitro*, and *in-silico* studies

Balasaheb D. Vanjare [a], Nam Gyu Choi [a], Prasad G. Mahajan [b], Hussain Raza [c], Mubashir Hassan [d], Yohan Han [c], Seon-Mi Yu [c], Song Ja Kim [c], Sung-Yum Seo [c], Ki Hwan Lee [a,*]

[a] Dept. of Chemistry, Kongju National University, Gongju, Chungnam 32588, Republic of Korea
[b] Vidya Pratishthan's Arts, Science & Commerce College, Vidyanagari, Baramati, Maharashtra 413133, India
[c] Department of Biological Science, Kongju National University, Gongju, Chungnam 32588, Republic of Korea
[d] Institute of Molecular Biology and Biotechnology, The University of Lahore, 54590, Pakistan

ARTICLE INFO

Keywords:
1,3,4-oxadiazole
Cytotoxicity
Dynamic simulation
Melanin content
Molecular docking
Tyrosinase inhibitor

ABSTRACT

In this research work, we have designed and synthesized some biologically useful of 1,3,4-Oxadiazoles. The structural interpretation of the synthesized compounds has been validated by using FT-IR, LC-MS, HRMS, ^{1}H NMR and ^{13}C NMR techniques. Moreover, the *in-vitro* mushroom tyrosinase inhibitory potential of the target compounds was assessed. The *in-vitro* study reveals that, all compounds demonstrate an excellent tyrosinase inhibitory activity. Especially, 2-(5-(2-methoxyphenyl)-1,3,4-oxadiazol-2-ylthio)-*N*-phenylacetamide (IC_{50} = 0.003 ± 0.00 μM) confirms much more significant potent inhibition activity compared with standard drug kojic acid (IC_{50} = 16.83 ± 1.16 μM). Subsequently, the most potent five oxadiazole compounds were screened for cytotoxicity study against B16F10 melanoma cells using an MTT assay method. The survival rate for the most potent compound was more pleasant than other compounds. Furthermore, the western blot results proved that the most potent compound considerably decreased the expression level of tyrosinase at 50 μM ($P < 0.05$). The molecular docking investigation exposed that the utmost potent compound displayed the significant interactions pattern within the active region of the tyrosinase enzyme and which might be responsible for the decent inhibitory activity towards the enzyme. A molecular dynamic simulation experiment was presented to recognize the residual backbone stability of protein structure.

1. Introduction

Tyrosinase (EC 1.14.18.1) is a copper encompassing metalloenzyme plays an influential part in the biosynthesis of melanin from tyrosine with the help of melanogenesis practice.[1] It is mostly found in animals, microorganism territories and plants. The melanogenesis process was carried out in two steps in which tyrosinase act as a catalyst.[2] Initially, the ortho diphenol (O-diphenol) conversion takes place from monophenol by hydroxylation. Secondly, the ortho diphenol gets converted into ortho quinone (O-quinone) by oxidation process and the established quinone product is extremely reactive species for the synthesis of the melanin pigments.[3,4] The formation of melanin in skin symbolizes the major protection action against exposure to UV radiation, excessive melanin formation can affect other skin diseases including solar lentigo, cancer, melasma, inflammatory melanoderma, flecks, age spots and ephelis.[5,6] To defeat this challenge, there is a necessity of a decent tyrosinase inhibitor which can regulate the melanin synthesis process. Hence, it is imperative to synthesize and development of tyrosinase inhibitor that can regulate the synthesis of melanin in the human body. Over recent decades, there have been findings of numerous tyrosinase inhibitors, but a few display adequate strength and reliability in the use in medicinal and food industries. In this perspective, heterocyclic compounds for instance, triazole, triazolothiadiazole, thiazole, sulfonamides and quinolines tender attracting class of tyrosinase inhibitors. But among all tyrosinase inhibitors, azole framework has been described by high potency.[7–10]

Oxadiazole is a group of the heterocyclic compound belongs to the azole family. It holds two carbon, two nitrogen and one oxygen atom associated together within a five-membered ring. It exists in four forms (isomers) namely, 1,2,3-oxadiazole, 1,2,4-oxadiazole, 1,2,5-oxadiazole and 1,3,4-oxadiazole, respectively which is shown in Fig. 1.[11] Among all, 1,3,4-oxadiazole has developed a vital creation pattern for the

* Corresponding author.
E-mail address: khlee@kongju.ac.kr (K.H. Lee).

https://doi.org/10.1016/j.bmc.2021.116222
Received 18 November 2020; Received in revised form 12 May 2021; Accepted 13 May 2021
Available online 21 May 2021

expansion of the novel drugs and have more ability to undergo a different type of chemical reactions which made them more important for the development of the new molecule.[12] Therefore, it has been spotted that different azoles and its derivatives have earned additional appreciation for their bioactive nature.[13,14] Fig. 2 illustrates several leading clinical drugs which holds a 1,3,4-oxadiazole core structure. Likewise, compounds comprising oxadiazole core demonstrating a broad range of biological activity for instance, anti-inflammatory, antifungal, antiviral, an alkaline phosphatase inhibitor, antihypertensive, anticonvulsant, antidiabetic, anticancer, and tyrosinase inhibition properties.[15–18] Additionally, oxadiazole acquires significant competence as a tyrosinase inhibitor and several of them examined oxadiazole correspondents have been proven to be more effective inhibitors when an associated with standard drugs.[19]

In this research work, we report the multi-step synthesis of hybrid molecules, spectroscopic characterization, mushroom tyrosinase inhibition assay, molecular docking, and dynamic simulation studies of novel 1,3,4-oxadiazole comprising scaffolds. Molecular modelling and enzyme inhibition studies revealed a terrific association with the experimental findings.

2. Results and discussion

2.1. Chemistry

2.1.1. Design approach, synthesis, and characterization

In this research work, we have systematically synthesized twelve novel 1,3,4-oxadiazole founded compounds by modifying the several structural aspects of the previously described tyrosinase inhibitors.[20,21] The innovative structural aspects constructed in our objective compounds have been displayed in Fig. 3. From the literature survey, it has been noticed that Lam et al., and co-workers successfully employed numerous 3,5-substituted oxadiazole-2-thione compounds as a tyrosinase inhibitor. From the results, it has been observed that the 3-position nitrogen atom was substituted with diverse cyclic amino groups in a 1,3,4-oxadiazole-2(3H)-thiones which exhibit a good tyrosinase inhibitory activity varies from 0.87 to 1.49 μM, compared with standard drug kojic acid having IC_{50} value 9.18 ± 0.28 μM.[20] In which, we have replaced the 3-position substation to the second position, and 5-position naphthyl group to un/substituted phenyl group in 1,3,4 oxadiazole framework. Similarly, Bandar et al., and co-workers effectively synthesized some *N*-{3-[3-(9-methyl-9H-carbazol-3-yl)-acryloyl]-phenyl}-benzamide/amide compounds as a tyrosinase inhibitor with IC_{50} value ranges from 14.01 to > 100 μM when equated with kojic acid (IC_{50} = 16.22 ± 1.74 μM).[21] Later, we have founded on the Bioisosterism auxiliary assumption, we have unified two distinct scaffolds to establish another platform which was further utilized for tyrosinase inhibition study.

The essential 1,3,4-oxadiazole compounds **9(a-l)** were synthesized by following synthetic routes A/B/C as presented in Scheme 1. Firstly, in synthetic route A, different substituted and unsubstituted benzoic acid compounds **1(a-c)** were converted into its corresponding ester compounds **2(a-c)** by the esterification reaction. In which the acid compounds were treated with ethyl alcohol and in presence of concentrated sulphuric acid. Secondly, the converted phenyl ester compounds **2(a-c)** were converted into hydrazide compounds **3(a-c)**, by the reaction of hydrazine hydrate in ethanol at reflux condition, the substituted hydrazide compounds **3(a-c)** were afforded with 70–80% yield. Later, un/substituted 5-phenyl-1,3,4-oxadiazole-2-thiol compounds **5(a-c)** were synthesized in two-step reaction. In which the hydrazide compounds **3(a-c)**, treated with carbon disulphide (CS_2) during the basic condition to form its open ring type of corresponding hydrazide salt **4(a-c)**. Afterwards, the hydrazide salt compounds **4(a-c)** was taken as such for cyclisation process by treating with water in heating condition to form corresponding cyclised un/substituted 5-phenyl-1,3,4-oxadiazole-2-thiol compounds **5(a-c)** with 65–75% yield. Additionally, in synthetic route B, various 2-chloro-*N*-phenyl-halogen un/substituted acetamide compounds **8(a-d)** were synthesized by following our previously published article.[2] Finally, the route C signifies the coupling reaction among the thiol and alpha-chloro-*N*-phenylacetamide functionality in presence of weak base potassium carbonate (K_2CO_3) in DMF to form a corresponding un/substituted *N*-phenyl-2-(5-phenyl-1,3,4-oxadiazol-2-ylthio) acetamide compounds with 80–95% yield.

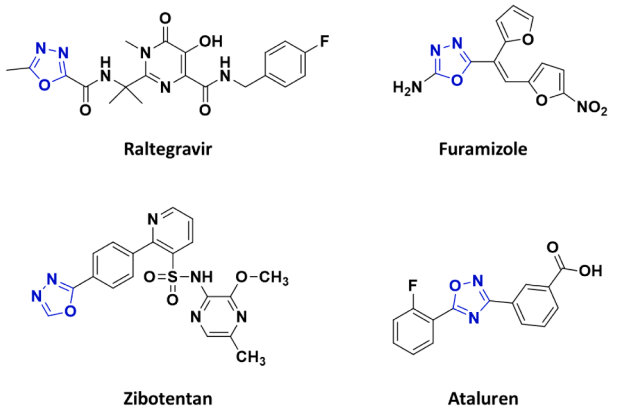

Fig. 2. Drugs with 1,3,4-oxadiazole core structure.

The characterization of the synthesized target compounds **9(a-l)** was accomplished by using ^{1}H NMR, ^{13}C NMR, LC-MS, HRMS, and FT-IR techniques. The structural elucidation of the compound **9e** is disused in details. The compound **9e** was acquired a white solid in 85% yield, possessing melting point around 138–142 °C. The molecular mass of the synthesized compound was identified by its molecular ion peak at 342.2 (M+1) in its LC-MS spectra. Besides, the number of proton and type of proton has been evaluated using ^{1}H NMR spectroscopy method. In which, the highly deshielded peak was observed for an amide proton at δ 10.44 (s, 1H). Also, the aromatic benzoyl group present in compound **9e** was appeared by its different signals at 7.62–7.57 (m, 2H), 7.34 (dd, J = 10.8, 5.1 Hz, 2H) and 7.09 (br.t, J = 7.4 Hz, 1H). Likewise, the numerous signals of 2-methoxy phenyl unit substituted at 5-position in 1,3,4-oxadiazole core were appeared at 7.55 (dt, J = 7.7, 1.3 Hz, 1H), 7.50 (t, J = 7.9 Hz, 1H), 7.45 (dd, J = 2.5, 1.5 Hz, 1H) and 7.20 (ddd, J = 8.0, 2.6, 1.2 Hz, 1H). Apart from the aromatic region, the compound **9e** acquire two signals for the aliphatic region comprising for methoxy and methylene groups appeared at 3.83 (s, 3H) and 4.36 (s, 2H) respectively. Also, the carbon skeleton of the synthesized compound **9e** was systematically validated using the ^{13}C NMR spectrum. Compound **9e** comprises amide functionality in which the carbonyl carbon signal has been detected at δ

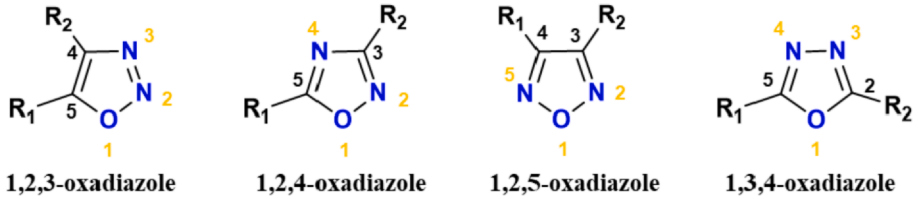

Fig. 1. Four different isomers of oxadiazole.

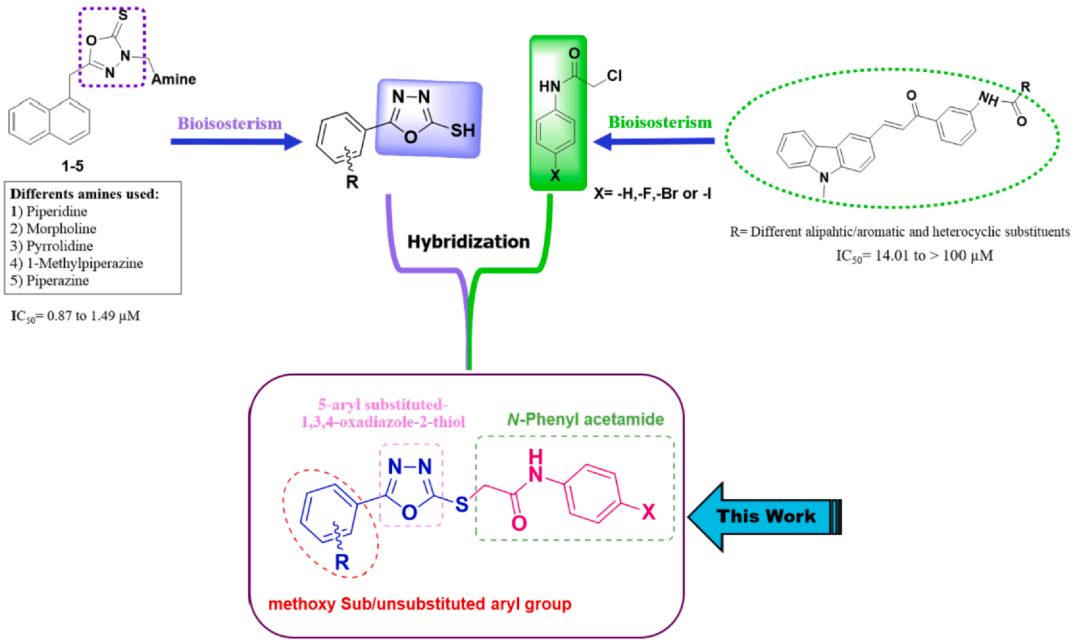

Fig. 3. Fragment-originated approach of proposed tyrosinase inhibitors.

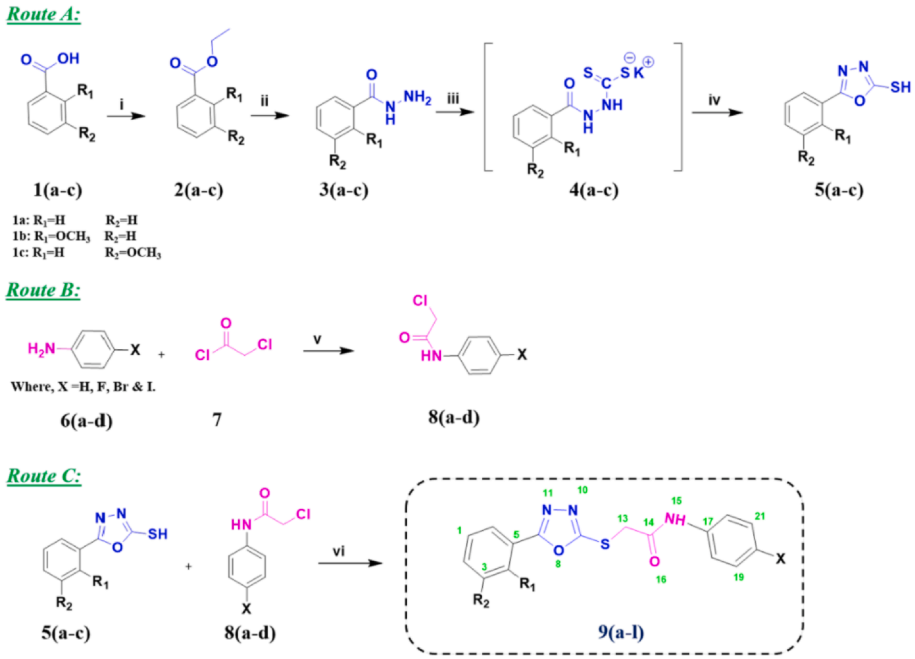

Scheme 1. Synthetic routes (A/ B & C), reagents and conditions; i) Ethanol, conc. H_2SO_4, reflux; ii) hydrazine hydrate, ethanol, reflux; iii) carbon disulphide (CS_2), ethanol, reflux 8 h; iv) water, reflux 4–5 h; v) triethyl amine, dichloromethane, 0–5 °C. vi) potassium carbonate, dimethyl formamide, ambient temperature.

165.5 (C-14). Furthermore, the formation of the 4,5-substituted 1,3,4-oxadiazole framework has been approved by the formation of two quaternary carbon which is observed at δ 165.3 (C-9) and 163.9 (C-7), respectively. Similarly, the compound involves two aromatic benzene rings also contains three quaternary carbon and are their signal appeared at δ 160.1 (C-4), 118.5 (C-5), and 139.1 (C-17) and the remaining aromatic signals appeared δ 131.2 (C-2), 129.3 (C-21 & C-19), 124.6 (C-20), 124.17 (C-1), 119.6 (C-18 & C-22), 119.1 (C-6), 111.6 (C-3) correspondingly. Moreover, the two aliphatic signals for methoxy and methylene group appeared at 55.9 (C-24) and 37.3 (C-13) present in respective compound **9e**. To validate different functional characteristics, vibrational studies of the molecules were analysed through FT-IR spectroscopy. The significant bands appeared in IR spectrum at υ 3268 (Ar-**NH**CO-), 3057 (aromatic SP^2 **C—H**), 2927 (SP^3 **C—H**), 1660 (Ar-NH-**CO**-), 1601, 1547 (aromatic **C═C** Bending), 1443 (SP^3 **C—H**, bending), 1176 (Ar-**O-CH**$_3$); 704.

The different substituents attached to the synthesized 1,3,4-oxadiazole compounds **9(a-l)** are listed in Table 1.

2.1.2. *In-Vitro tyrosinase activity and structural activity relationship (SAR)*

Herein, the synthesized novel heterocyclic compounds **9(a-l)** were screened for their mushroom tyrosinase inhibitory capability. All these compounds **9(a-l)** displayed exceptionally good tyrosinase inhibitory activity ranging from 0.003 ± 0.00 to 0.396 ± 0.01 µM, when

Table 1
Structures of the synthesized 1,3,4-oxadiazole compounds **9(a-l).**

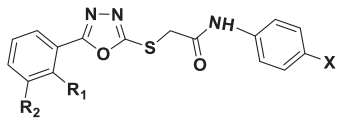

Sr. No	Compound	-R_1	-R_2	-X
1	**9a**	-H	-H	-H
2	**9b**	-H	-H	-F
3	**9c**	-H	-H	-Br
4	**9d**	-H	-H	-I
5	**9e**	–OCH_3	-H	-H
6	**9f**	–OCH_3	-H	-F
7	**9g**	–OCH_3	-H	-Br
8	**9h**	–OCH_3	-H	-I
9	**9i**	-H	–OCH_3	-H
10	**9j**	-H	–OCH_3	-F
11	**9k**	-H	–OCH_3	-Br
12	**9l**	-H	–OCH_3	-I

differentiated with the standard drug kojic acid (IC_{50} = 16.832 ± 1.16 μM). However, certain compounds involving; **9f, 9h, 9i & 9j**, demonstrate good inhibitory activity. But among the series **9(a-l),** compound **9e** believed to be an extremely active tyrosinase inhibitor than standard drug kojic acid. The accomplished inhibitory activity in a molecule is caused by the participation of the entire molecule, yet a limited SAR study was simplified by the existence of the different substituents in corresponding 1,3,4-oxadiazole compounds.

All the target compounds **9(a-l)** consist of 2-(1,3,4-oxadiazol-2-ylthio)-*N*-phenylacetamide as a fundamental framework. In which the 5-postion of the 1,3,4-oxadiazole were substituted with various aromatic phenyl groups for instance, phenyl group in **9(a-d)**, 2-methoxy phenyl in **9(e-h)** and 3-methoxy phenyl in **9(i-l)**, correspondingly. Also, the 4-position of the *N*-phenyl acetamide were unsubstituted or substituted with different halogens (Such as, -F, -Br and -I) which is shown in Scheme 1. Furthermore, the target compound **9a** (IC_{50} = 0.231 ± 0.09) acquire no substituent, while **9b** (IC_{50} = 0.396 ± 0.09), **9c** (IC_{50} = 0.039 ± 0.01) and **9d** (IC_{50} = 0.085 ± 0.08) hold fluoro, bromo and iodo halogen atoms as shown in Table 1. All these four compounds **9(a-d)** exhibit virtuous inhibitory activity as matched to the standard drug kojic acid (IC_{50} = 16.83 ± 1.16). Moreover, the tyrosinase inhibitory activity for un-substituted **9a** and fluoro substituted derivative **9b** was not that much effective as compared with the compounds bearing bromo **9c** and iodo **9d** group at para position concerning to *N*-phenyl acetamide functionality. Since, as the size of the halogen atom increases at *para*-position, the interaction with enzyme improves as a result pointing decent inhibitory activity.

Also, as presented in Table 1, the 5-position of the 1,3,4-oxadiazole heterocyclic ring was substituted with the *ortho*-methoxy phenyl unit and the *N*-phenyl acetamide functional group holds no substituent, fluoro, bromo or iodo groups at para position in respective target compounds **9(e-f)**. Herein, all the compounds present extremely great inhibition rate as equated with compounds **9(a-d)**. It suggests that the *ortho*-substituted methoxy phenyl group present in the respective target compounds create a good interaction pattern with an enzyme which causes to exhibit good inhibition rate. Nevertheless, among the *ortho*-methoxy substituted compounds **(9e, 9d, 9e & 9f)**, the compound **9e** (IC_{50} = 0.003 ± 0.00 μM) demonstrate excellent activity because it does not hold any substituent concerning to the *N*-phenyl acetamide functionality. Whereas other compounds (**9f**, **9g** and **9h**) acquires halogen unit at *para*-position indicates reduced inhibitory activity. The result indicates that, as the halogen size increases the interaction with enzyme becomes lower, however these findings are opposite in accordance with the compounds **9(a-d)**.

Similarly, when the inhibitory potential of *meta*-substituted methoxy phenyl compounds, **9i** (IC_{50} = 0.019 ± 0.00 μM), **9j** (IC_{50} = 0.027 ± 0.10 μM), **9k** (IC_{50} = 0.145 ± 0.09 μM) and **9l** (IC_{50} = 0.088 ± 0.10 μM) compared with **9e-9h** (Table 2). It has been observed that, the activity trend was almost similar for compound **9(e-h)** and **9(i-l)**, but it was irregular in **9(a-h)**. It suggests that *ortho*-substituted strong electron-donating unit found to be more effective to enhance the inhibition rate than *meta*-substituted or unsubstituted compounds at 5-position substituted phenyl group in an 1,3,4-oxadaizole core. Additionally, however, oxadiazole compounds **9i**, **9j**, **9k** and **9l** holds same functionality expect the substitution at para position with regards to *N*-phenyl acetamide functional group. In which **9i** possess no substituents at para position relating to acetamide functionality while **9j**, **9k** and **9l** comprises fluoro, bromo and iodo substituents. The results suggest that, in absence of halogen substituent in the oxadiazole compounds presents excellent interaction pattern with the enzyme but it is practically opposite in case para substituted halogen atoms.

In conclusion, from the structural activity relationship assessment, it was spotted that ortho and *meta*-methoxy phenyl group when substituted at 5-position in 1,3,4-oxadiazole compounds reveals comparable activity trend in presence or absence of halogen groups regarding amide functionality. While, in case of only aromatic benzene substituted group in 1,3,4-oxadiazole core reveals varying activity style. Also, it can be asserted from the docking study that (Fig. 8), methoxy phenyl containing compounds **9(e-l)** exhibit good binding energy pattern than un-substituted methoxy compounds **9(a-d)** at 5-position in 1,3,4-oxadiazole core. The activity movement for synthesized 1,3,4-oxadiazole compounds **9(a-l)** are arranged as per their interaction relationship with enzyme explored through *in-vitro* evaluation analysis, for example **9e>9f>9i>9h>9j>9c>9g>9d>9l>9k>9a>9b** (IC_{50} values are arranged in Table. 2).

2.2. Biology analysis

2.2.1. Kinetic mechanism

Kinetic analysis was accomplished to check the mechanism of most potent compound **9e**, the compound was nominated based on IC_{50} outcomes. The inhibition kinetics of **9e** on the mushroom tyrosinase was analysed using the Lineweaver-Burk plot. The outcomes are presented in Fig. 4**A**, showed that the plots of 1/V versus 1/[S] gave a series of straight lines which intersected within the second quadrant. These data showed **9e** inhibit the tyrosinase in a non-competitive manner. The K_i value was obtained from the (Fig. 4**B**) of slope against the concentrations of inhibitor. The kinetic results are presented in Table 3. (Kinetic parameter table).

2.2.2. Effect of compound 9e on the expression of tyrosinase

In order to explore the impact of the compound **9e** over tyrosinase expression, we have organized a western-blot experimental study. In which the most potent compound **9e** were treated with the B16F10 cells at various concentrations including, 10, 20, 30 and 50 μM independently. Herein, α-MSH was employed as a melanogenic inducers.[22] The results are shown in Fig. 5**A**, designates that α-MSH significantly induces

Table 2
Various substituents present to target compounds **9(a-l)** and its IC_{50} value for tyrosinase activity. (SEM = Standard error of the mean; values are expressed in mean ± SEM).

Compound	Tyrosinase activity IC_{50}±SEM (μM)	Compound	Tyrosinase activity IC_{50}±SEM (μM)
9a	0.231 ± 0.09	**9g**	0.046 ± 0.88
9b	0.396 ± 0.09	**9h**	0.023 ± 0.89
9c	0.039 ± 0.01	**9i**	0.019 ± 0.00
9d	0.085 ± 0.08	**9j**	0.027 ± 0.10
9e	**0.003±0.00**	**9k**	0.145 ± 0.09
9f	0.018 ± 0.08	**9l**	0.088 ± 0.10
Kojic Acid (Standard)		**16.832±1.16μM**	

SEM = Standard error of the mean; values are expressed in mean ± SEM.

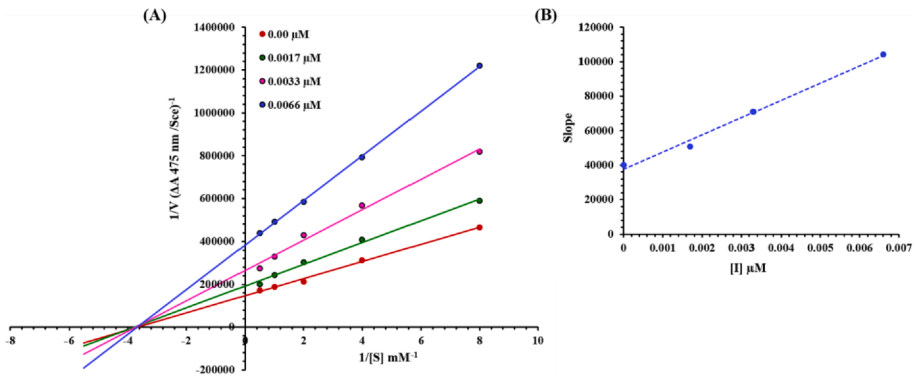

Fig. 4. Lineweaver–Burk plots for the inhibition of tyrosinase in the presence of compound **9e**. **(A)** Concentrations of **9e** were 0.00, 0.0017, 0.0033 and 0.0066 μM, respectively. Substrate L-DOPA concentrations were 0.125, 0.25, 0.5, 1 and 2 mM, respectively. **(B)** Slope against **9e** concentrations. The lines were drawn using linear least squares fit.

Table 3
Kinetic parameters of **9e** on mushroom tyrosinase inhibition for L-DOPA activity.

Concentration (μM)	V_{max} (ΔA /*Sec*)	K_m (mM)	Inhibition Type	K_i (μM)
0.00	5.818×10^{-6}	0.25	Non-Competitive	0.0031
0.0017	4.970×10^{-6}	0.25		
0.0033	3.636×10^{-6}	0.25		
0.0066	2.273×10^{-6}	0.25		

V_{max} is the reaction velocity, K_m is the Michaelis-Menten constant, K_i is the EI dissociation constant.

the tyrosinase expression as equated with the control. Also, when the compound **9e** incubated with α-MSH at 10 μM, the tyrosinase expression was slightly decreased. Nevertheless, a drastic shift was detected after the concentration was raised between 20 and 30 μM and then relatively stable at 50 μM as shown in Fig. 5**B.** These results exhibit that 1,3,4-oxadiazole compound **9e** drastically diminished α-MSH stimulated melanin synthesis.

2.2.3. Melanin contents assay of compound 9e

Melanin plays an important role in determining the colour of the mammalian skin and for protection from UV radiation. Also, it is very well known that α-melanocyte stimulating hormone (α-MSH) primarily utilized for the activation of the melanogenesis process.[23–25] Hence, we have utilized α-MSH as a melanogenic inducer. Furthermore, to recognize the content of the melanin in B16F10 cells, initially, the cells were preserved with α-MSH followed by a co-treatment with an 1,3,4-oxadiazole compound **9e** at distinct concentrations comprising 10, 20, 30, and 50 μM, respectively. The prepared samples were incubated with a period of 24 h. Afterwards, the absorbance (optical density) was measured for each sample at 470 nm, to determine the melanin formation inhibitory impact of the compound **9e**. As presented in Fig. 6**,** it exposes that compound **9e,** passionately and effectively diminishes the content of the melanin as equated with the control. The oxadiazole derivative **9e** decreases the melanin contents to 16%, 62%, 77% and 78% at 10, 20, 30 and 50 μM concentrations relating to the α-MSH. Hence, it suggests that compound **9e** sharply reduces the melanin content present in α-MSH stimulated in B16F10 cells in a concentration dependant approach.

2.2.4. Cell viability

To develop a skin lighting agent or compound, it must have to accomplish the criteria that, it should be harmless to consume without any adverse effects. At present, there are several previously registered

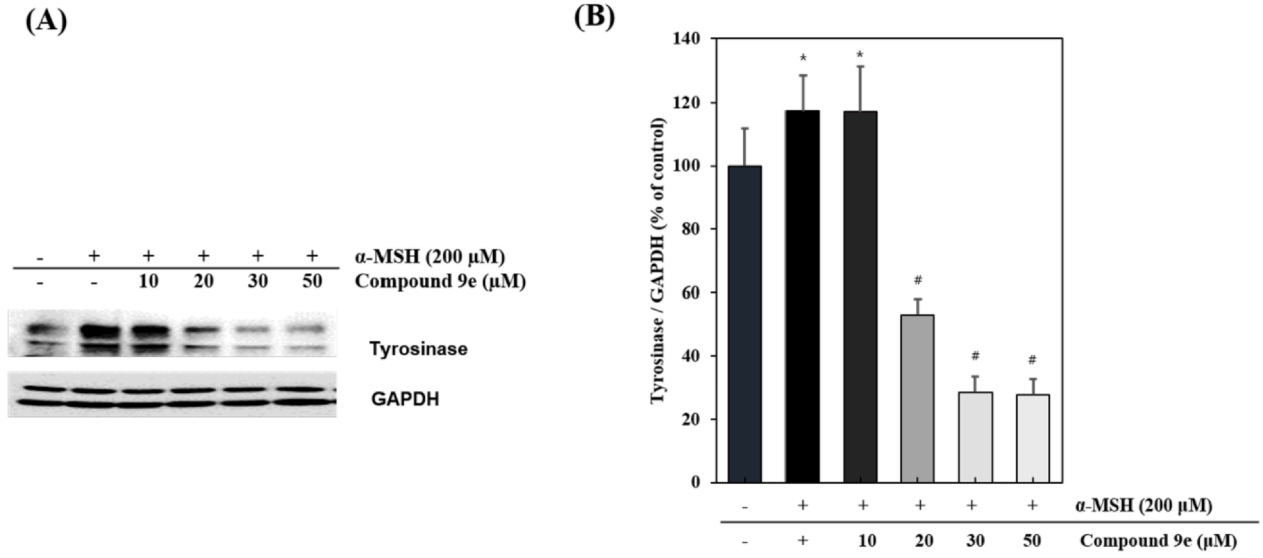

Fig. 5. The effects of compound **9e** on the α-MSH induced tyrosinase expression in B16F10 cells. Cells were exposed with or without α-MSH in the presence of different concentration of compound **9e** (10, 20, 30 & 50 μM) for 24 h. Tyrosinase expressions were determined by western-blot analysis using GAPDH as loading control (A) α-MSH increased the expression of tyrosinase in comparison to normal control (B) Compound **9e** reduced the α-MSH induced expression of tyrosinase. The asterisks signify the considerable variation among the columns: $^{*}P < 0.05$; and $^{\#}P < 0.001$.

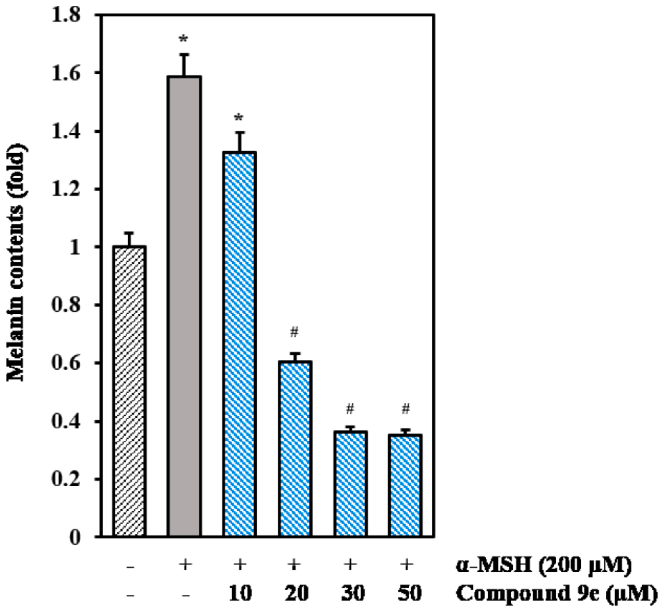

Fig. 6. The inhibitory effect of **9e** in B16F10 cells. The melanin content of the human B16F10 cells treated with different concentrations of **9e** (10, 20, 30 & 50 μM). Data are presented as mean ± SD; $n = 3$; * $P < 0.05$; # $P < 0.001$; compared with the control groups.

skin whitening agents (tyrosinase inhibitors) are accessible in the market including, hydroquinone, PTU, arbutin and kojic acid.[2,26] Even though, most of the pharmaceutical companies and research institutes are engaged to synthesize and develop various tyrosinase inhibitors. Herein, we have synthesized and developed twelve novel tyrosinase inhibitors which show decent inhibitory activity. However, amongst all, we have selected the first five potent compounds **(9e, 9f, 9h, 9i & 9j)** for the cell viability analysis. The cell viability study was conducted by following our previously published article. In which the cytotoxicity study was conducted using a MTT assay method on B16F10 cells. Initially, the B16F10 cells were cultivated in most five potent compounds **(9e, 9f, 9h, 9i & 9j)** for 24 h (hrs) at various concentrations including 1, 5, 10, 20, 30, 40 and 50 μg/mL using DMSO as a solvent and the cell viability was determined. From cell viability results (Fig. 7) demonstrate compounds **9e, 9f & 9h** shows cell viability more than 80% even at high concentration 50 μg/mL. But compound **9i & 9j** show nontoxic behaviour up to 10 μg/mL but afterwards it acted as toxic to the B16F10 cells. Therefore, among all compounds compound **9e** demonstrates most promising potent inhibitory activity as well as exhibit good survival rate against B16F10 cells. Therefore, in future compound **9e** could be treated as outstanding tyrosinase inhibitor in the vicinity of the pharmaceutical chemistry for the improvement of the new drug.

2.3. In-Silico analysis

2.3.1. Mushroom tyrosinase structural assessment

Mushroom tyrosinase, a copper-containing enzyme comprises 391 residues.[27] The detailed structure analysis target protein showed that it consists of 39% α-helices, 14% β-sheets and 46% coils. The X-ray diffraction study confirmed its resolution 2.78 Å, R-value 0.238 and unit cell crystal dimensions such as coordinates length and angles. The Ramachandran plots and values indicated that 95.90% of protein residues were present in the favoured region and 100.0% residues were lie in the allowed region showed in **Fig. S73**. The Ramachandran graph values showed the good accuracy of phi (φ) and psi (ψ) angles among the coordinates of receptor and most of the residues were plunged in acceptable region.

2.3.2. Molecular docking analyses

The best way to study the binding conformation of ligands against target protein is through molecular docking analysis and which was conducted by following our previously reported articles with little modifications.[2,6,24,28–31] The docked complexes of the synthesized compounds **9(a-l)** against tyrosinase were analysed based on lowest binding energy values (Kcal/mol) and hydrogen/hydrophobic interaction pattern. Results showed that all the ligands **9(a-l),** exhibited good docking energy values and showed their interaction within active region of target protein (Fig. 8). The docking energy values of all the docking

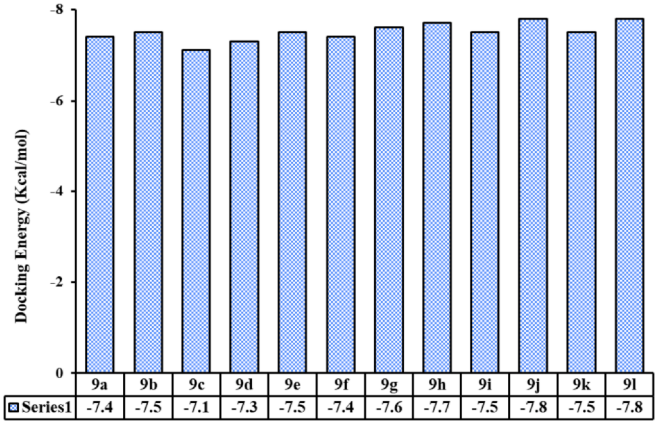

Fig. 8. Energy graph of synthesized compounds.

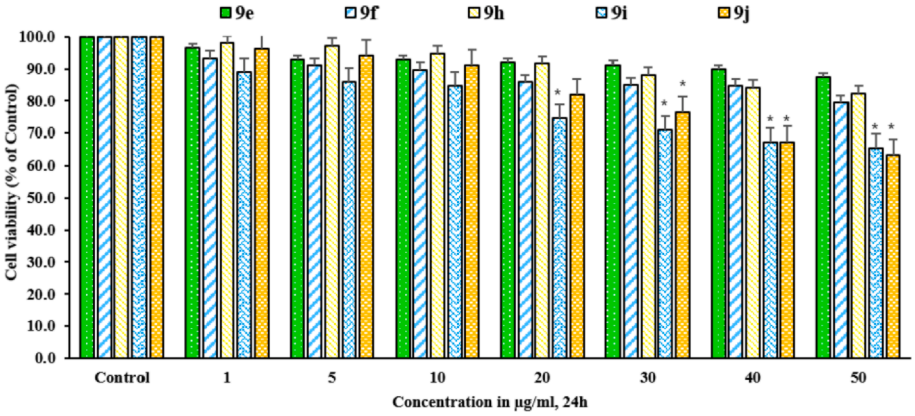

Fig. 7. Cell viability measurement employing MTT assay method. Cells were untreated (control) or treated with most potent compounds **9e, 9f, 9h, 9i & 9j** at various concentrations (1, 5, 10, 20, 30, 40, 50 μg/mL) in DMSO for 24 h. (*$P < 0.05$).

complexes was calculated by using equation (1).

$$\Delta G\ binding = \Delta G\ gauss + \Delta G\ repulsion + \Delta G\ hbond + \Delta G\ hydrophobic + \Delta G\ tors \quad (1)$$

Here, ΔG gauss: attractive term for dispersion of two gaussian functions, ΔGrepulsion: square of the distance if closer than a threshold value, ΔGhbond: ramp function also used for interactions with metal ions, ΔGhydrophobic: ramp function, ΔGtors: proportional to the number of rotatable bonds. In docking energy results compounds selected as best having more than 2.5 kcal/mol energy value different compared to other compounds. The standard error for Auto dock is reported as 2.5 kcal/mol.[32] Present docking results justified that the energy value difference among all docking complexes were lower than standard error value. Therefore, based on both *in-vitro* and *in-silico* docking energy results, **9e** was ranked as best ligand which showed good inhibitory potential against targeted enzyme as compared with other compounds. Also, the binding affinity of the standard drug kojic acid (-5.7 kcal/mol) was equated with the binding affinities of all the synthesized compounds, in which it has been noticed that all the target compounds exhibit respectable binding energy than kojic acid.[24] Although, the basic nucleus of all the synthesized compounds were the same, therefore most of the ligands possess good efficient energy values and have no big energy fluctuations difference.

2.3.3. Binding pocket and ligands binding conformations

The binding pocket analysis showed that **9e** were confined in the active region of target protein nearby copper metal. All the docked structures were superimposed to check the binding configuration of all ligands in the active region of mushroom tyrosinase. Results showed that the synthesized ligands were bind in the binding pocket having at least similar conformational pattern. All ligands showed little deviation around their axis in configuration shape. The aromatic benzene ring and an oxygen atom of the carbonyl functionality appear in target compound **9e** proved their binding pattern in the opening gate of binding pocket. Whereas the presence of different incorporated functional moiety showed their attachment inside the binding pocket near the copper metal (Fig. 9**A, B**). The **9e**-docking complex showed that incorporated functional group showed its penetration inside the binding pocket and may have potential to binds with active site residues of target protein. This incorporation may result in suitable configuration and conformation to ligands to be fitted in the binding pocket of mushroom tyrosinase.

2.3.4. Hydrogen and hydrophobic binding interaction between 9e and target protein

The binding interaction showed that **9e** directly binds with active region residues of mushroom tyrosinase. The docking results showed that **9e** builds single hydrogen bond with His244 and one hydrophobic interaction with Met280, respectively. The carbonyl oxygen atom from a single hydrogen bond with His244 having good binding distance 1.88 Å. Similarly, methyl group was involved with Met280 by hydrophobic interaction with bond length 3.32 Å. Our incorporated functional moiety directly indulges with functional residues of target protein and have strong correlation with *in-vitro* results. Literature study also justified that these binding pocket residues are significant in downstream signaling pathways.[4,27,33] The graphical depiction of **9e** docking complex is mentioned in Fig. 10 and all other complexes in Supplementary data **Figs. S61–S72.**

2.3.5. Root mean square deviation and fluctuation analysis

The RMSD results showed that protein backbone deviation and fluctuations behaviour in the simulation time frame from 0 to 5000 ps. The **9e** docked complex (blue) graph line depicted good stable and steady behaviour throughout the simulation period (Fig. 11). Initially, graph line showed increasing fluctuations to attain stability with RMSD value range form 0.1–0.27 nm from simulation time 0–500 ps. From time 500–1000 ps, **9e** graph line remained static having stable RMSD value 0.15 nm. From 1000 to 5000 ps docked complexes showed similar stable behaviour with minute fluctuations pattern. The observed results showed that our complex showed good stable behaviour after binding with newly synthesized ligands.

Also, Fig. 12 showed the stability of **9e** docking structure dynamically fluctuated from residues N to C terminus. The fluctuation peaks within loops region were observed at both terminus N and C-terminal regions.

2.3.6. Radius of gyration and solvent accessible surface area analyses

The structural compactness in protein docking complex was observed by radius of gyration (Rg). The stably folded proteins show the relatively steady value of Rg in equilibrium state whereas, in static phase it remains stable with little fluctuations and Rg valued also remained stable throughout the simulation time. The generated results depicted that Rg graph showed downward trend from 0 to 1000 ps with Rg value ranged from 2.0 to 2.04 nm. After that Rg graph line remained stable from 1000 to 4000 ps with constant Rg value 2 nm. From 4000 to 5000 ps again little fluctuation was observed, however, the Rg value remained stable in the simulation period (Fig. 13). The solvent-accessible surface areas (SASA) were also observed and shown in (Fig. 14). Results showed that the SASA values of **9e** docking complex were centered on 205–210 nm in the simulation time 0–5000 ps.

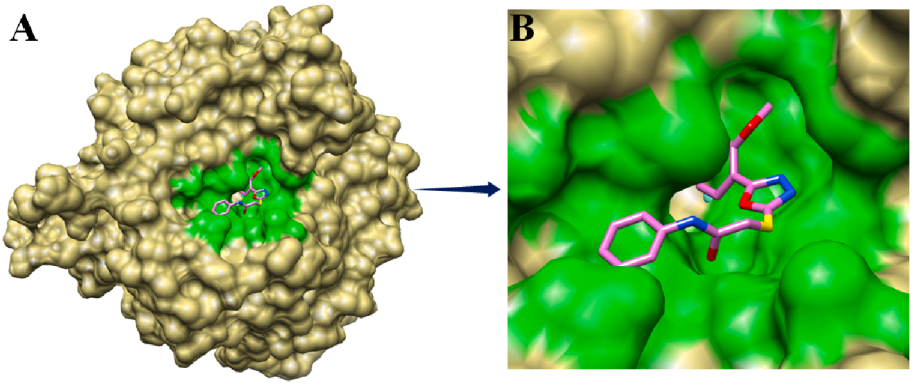

Fig. 9. A, B. Binding of ligands within active region of target protein. The receptor molecule is highlighted in grey colour in surface format. However, ligand is justified in purple colour.

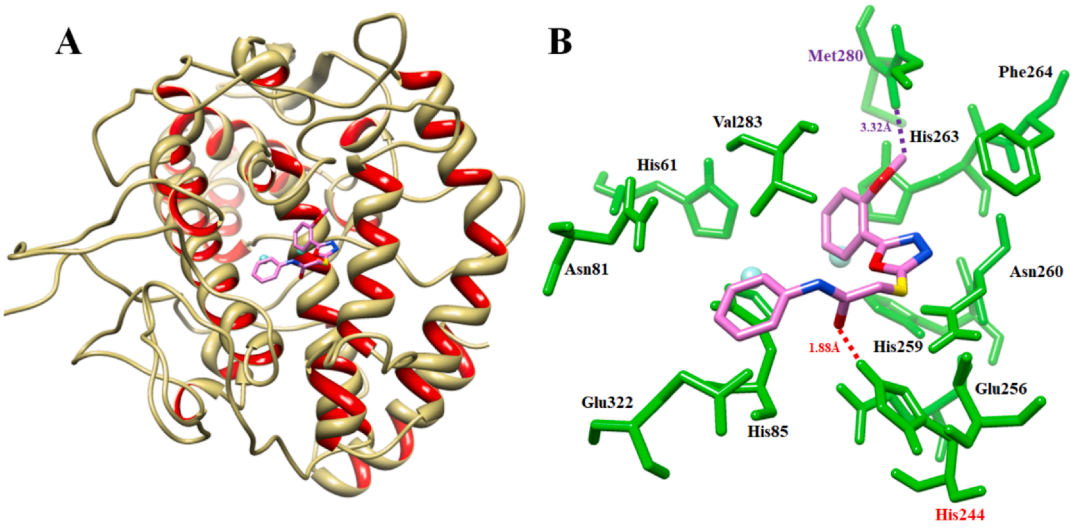

Fig. 10. Molecular docking interaction of **9e** with receptor molecule. A) The protein structure is represented in khaki and red colours in ribbon format while ligand is highlighted purple colour while their functional groups such as oxygen, amino and sulfur are showed in red, blue, and yellow colours, respectively. B) The interactive residues are justified in green colour whereas, amino acids involve in hydrogen bonds and hydrophobic interactions are labelled in red and dark blue, respectively. The dotted lines represent bond distances in angstrom (Å). Two copper ions are represented in light cyan circles.

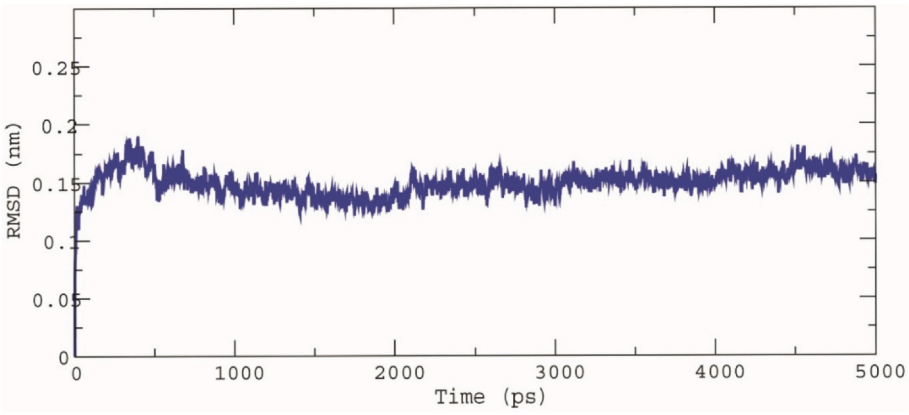

Fig. 11. RMSD graph of compound **9e**.

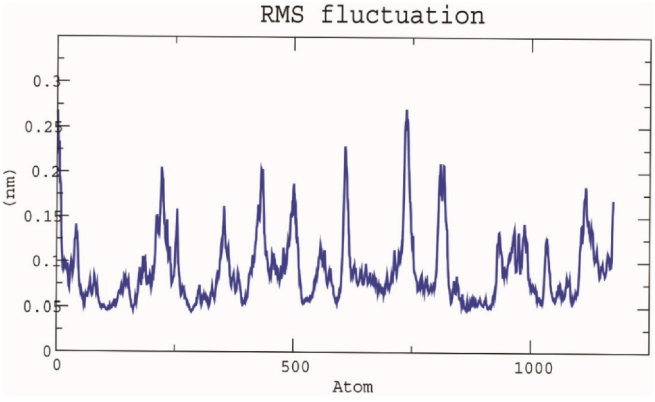

Fig. 12. RMSF graph of compound **9e**.

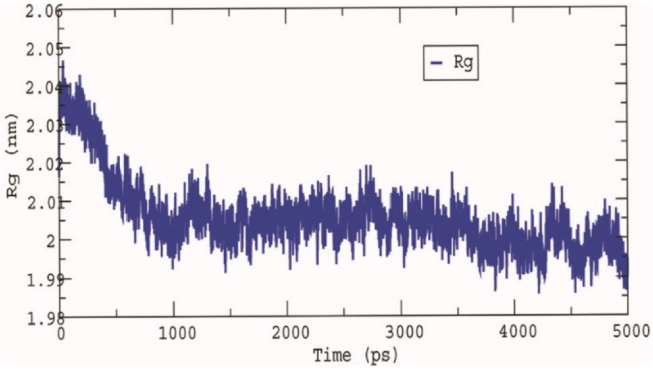

Fig. 13. Rg graph of compound **9e**.

3. Conclusion

To conclude, we have designed and synthesized twelve novel 1,3,4-oxadiazole compounds through multistep reaction pathway. The synthesis of the target compounds was initiated with different aromatic acid composites, which are converted into un/substituted 5-phenyl-1,3,4-oxadiazole-2-thiol molecule by employing multistep chemical reactions and ultimately it coupled with 2-chloro-*N*-phenyl-halogen un/substituted acetamide compounds to offer a target compounds **9(a-l)** with good yields. The structural elucidation of the target compounds was carried out *via* FT-IR, LC-MS, HRMS, ^{1}H NMR and ^{13}C NMR

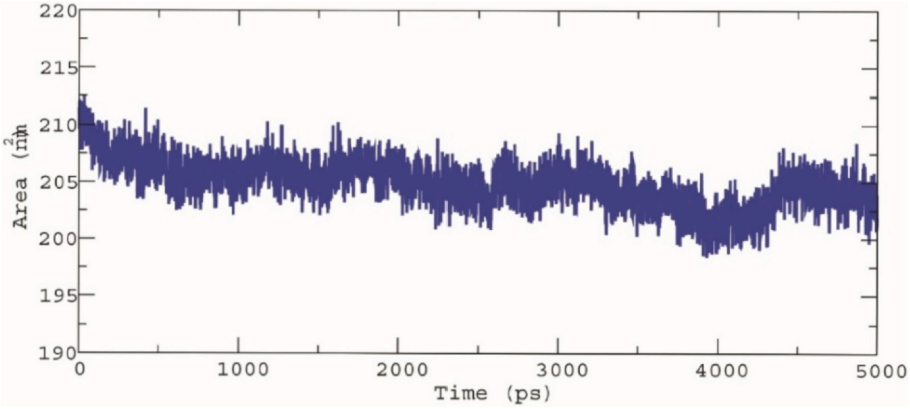

Fig. 14. SASA graph of compound **9e**.

practices. Furthermore, all the 1,3,4-oxadiazole compounds were evaluated against mushroom tyrosinase activity. The results showed that, all compounds **9(a-l)** present good inhibitory activity against mushroom tyrosinase enzyme than standard drug kojic acid. Mainly, compound **9e** seems to be extremely effective throughout the series. The inhibition kinetics for most potent compound **9e** was analysed by using Lineweaver-Burk plots and is found to be non-competitive. Subsequently, cell-based experiments were carried out on B16F10 melanoma cells, the results reveal that compound **9e** is non-toxic even at high concentration (0–50 μM) and confirms exceptional anti-melanogenic effect validated using western blot findings. Additionally, the most effective compound **9e** passionately associates with essential amino acid for example Met 280 and His 244 was proven by docking analysis. Also, the molecular dynamic simulation experiment was performed to recognize the residual backbone stability of protein structure. Overall, one can be concluded from the entire study that, all the synthesized novel 1,3,4-oxadiazole compounds were considered as a good therapeutic agent. Though, among the series compound **9e** served as a potent tyrosinase inhibitor and hence in future, it could be employed as a great contender of the drug in a medicinal field for the expansion of the new medication.

4. Materials and methods

4.1. Chemistry

The required chemicals were purchased from Sigma Aldrich (Munich, Germany) and Samchun chemicals (Daejeon, South Korea) and used without purification. ^{1}H NMR and ^{13}C NMR spectra were taken in $(CD_3)_2SO$ at 400 & 100 MHz spectrophotometers, by using a Bruker Avance (Germany). The chemical shift and coupling constant (*J*) values mentioned in ppm and Hz, respectively. The mass analysis (LC-MS) was recorded on 2795/ZQ2000 (waters) spectrometer and HRMS spectra was recorded on UHPLC/High Resolution Mass Spectrometer, Model: 1290 infinity II/ Triple TOF 5600 plus (USA). The FT-IR spectra were recorded on Frontier IR spectrophotometer (Perkin Elmer, USA). Melting points of the target compounds were determined in open capillary tubes and are uncorrected (Pittsburgh, PA, and USA). The melting points of the compounds **9(a-l)** were determined by using Fisher Scientific (USA) melting point instrument and are uncorrected. The improvement of the reactions was monitored by a thin layer chromatography (TLC) technique.

4.1.1. General synthetic procedure for the key intermediate (2a-2 g), (3a-3b) and (8a-8d):

The intermediate **2(a-b)**, **3(a-b)** and **8(a-d)** were prepared by following previously reported method.[2,34]

4.1.2. General synthetic procedure for the key intermediate 5(a-c):

The intermediate **5(a-c)** were synthesized by two step reaction. Firstly, to a 100 mL flask was added the intermediate compound **3(a-b)** (1 mmol) and milled potassium hydroxide (1.1 mmol) in ethanol (5 mL), stirred for 10 min under nitrogen atmosphere. Later, slowly added carbon disulphide (2 mmol) to the reaction mixture, solid will observed (if necessary, add ethanol) and heated to reflux for 4–5 h. The reaction progress was detected by using TLC technique. After completion of the reaction, the reaction mass was cooled to room temperature and concentrated under reduced pressure to afford a crude solid **4(a-d)**. The obtained crude solid was taken as such for further step.

The obtained crude intermediate **4(a-d)** was taken in water and heated to reflux at 70–80 °C for 7–8 h. After completion of the reaction, the reaction mixture was gradually brought to room temperature followed cooled to 0 to 5 °C. Then neutralised with 10% hydrochloric acid solution, the precipitated solid was filtered, and several times washed with cold water. The obtained solid was dried and used as it is for next step.

4.1.3. General procedure for the synthesis of the target compounds 9(a-l):

As displayed in Scheme 1**,** an intermediate compound **5(a-l)** (1 mmol) and potassium carbonate (1.5 mmol) in dimethylformamide (DMF) were stirred under nitrogen atmosphere at room temperature for 15–20 min. Afterwards, added intermediate 8**(a-d)** (1 mmol) to the above reaction mixture and stirred for 4–5 h. After completion of the reaction, ice cold water was added to the reaction mixture and stirred for 20 min (solid was obtained). The obtained solid was filtered and several times washed with cold water and dried. The acquired crude solid was purified by column chromatography skill, when eluting with the hexane and ethyl acetate as a solvents to afford a pure 1,3,4-oxadiazole compounds **9(a-l)** with an excellent yield.

*4.1.3.1. Synthesis of the N-phenyl-2-(5-phenyl-1,3,4-oxadiazol-2-ylthio) acetamide (**9a**).* White solid; isolated yield: 80%; $R_f = 0.65$ (*n*-hexane: ethyl acetate, 1:1); mp-141–145 °C. **Fig. S1:** ^{1}H NMR (400 MHz, $(CD_3)_2SO$) $\delta = 10.44$ (s, 1H), 7.99 – 7.95 (m, 2H), 7.69–7.53 (m, 5H), 7.37–7.30 (m, 2H), 7.12 – 7.06 (m, 1H), 4.36 (s, 2H). **Fig. S2:** ^{13}C NMR (100 MHz, $(CD_3)_2SO$) $\delta = 165.5, 165.3, 163.8, 139.0, 132.4, 129.8, 129.33, 126.8, 124.14, 123.4, 119.5$ and 37.3. **Fig. S3:** IR (KBr) cm^{-1}: 3267 (Ar-**NH**CO-), 2983 (SP^2 **C—H**), 2927 (SP^3 **C—H**), 1681 (Ar-NH-**CO**-), 1600, 1553 (aromatic **C═C** bending), 1474 (SP^3 **C—H,** bending), 1197 (Ar-**O-CH$_3$,**) 705. **Fig. S4:** LC-MS: 312 *m/z*. **Fig. S5:** HRMS (*m/z*): calculated (312.0801, M+H); observed (312.0805, M+1).

*4.1.3.2. Synthesis of the N-(4-fluorophenyl)-2-(5-phenyl-1,3,4-oxadiazol-2-ylthio) acetamide (**9b**).* Off-white solid; isolated yield: 82%; $R_f = 0.61$ (*n*-hexane: ethyl acetate, 1:1); mp-137–141 °C. **Fig. S6:** ^{1}H NMR (400 MHz, $(CD_3)_2SO$) $\delta = 10.50$ (s, 1H), 8.01 – 7.91 (m, 1H), 7.80 (d, $J = 7.4$

Hz, 1H), 7.69 – 7.52 (m, 3H), 7.52 – 7.30 (m, 3H), 7.22 – 7.11 (m, 1H), 4.19 (s, 2H). **Fig. S7:** ^{13}C NMR (150 MHz, $(CD_3)_2SO$) δ = 165.1, 164.8, 163.3, 158.9, 157.3, 135.0, 135.0, 132.0, 129.4, 126.3, 122.9, 121.0, 120.9, 115.9, 115.5, 115.3 & 36.6. **Fig. S8:** IR (KBr) cm^{-1}: 3269 (Ar-**NH**CO-), 3140 (aromatic SP^2 **C—H**), 2926 (SP^3 **C—H**), 1676 (Ar-NH-**CO**-), 1600, 1552 (aromatic **C═C** bending), 1473 (SP^3 **C—H**, bending), 1196 (Ar-**O-CH$_3$**); 705. **Fig. S9:** LC-MS: 330 *m/z*. **Fig. S10:** HRMS (*m/z*): calculated (330.0707, M+H); observed (330.0703, M+1).

*4.1.3.3. Synthesis of N-(4-bromophenyl)-2-(5-phenyl-1,3,4-oxadiazol-2-ylthio) acetamide (**9c**).* Grey solid; isolated yield: 81%; R_f = 0.63 (*n*-hexane: ethyl acetate, 1:1); mp-169–173 °C. **Fig. S11:** ^{1}H NMR (400 MHz, $(CD_3)_2SO$) δ = 10.58 (s, 1H), 7.96 (d, *J* = 7.2 Hz, 2H), 7.66 – 7.60 (m, 2H), 7.57 (d, *J* = 8.7 Hz, 3H), 7.52 (d, *J* = 8.9 Hz, 2H), 4.35 (s, 2H). **Fig. S12:** ^{13}C NMR (100 MHz, $(CD_3)_2SO$) δ = 165.6, 163.8, 163.7, 138.5, 132.5, 132.1, 129.8, 126.8, 123.4, 121.5, 115.7, & 37.2. **Fig. S13:** IR (KBr) cm^{-1}: 3322 (Ar-**NH**CO-), 2982 (aromatic SP^2 **C—H**), 2927 (SP^3 **C—H**), 1664 (Ar-NH-**CO**-),1599, 1527 (aromatic **C═C** bending), 1445 (SP^3 **C—H,** bending), 1198 (Ar-**O-CH$_3$**); 704. **Fig. S14:** LC-MS: 392 *m/z*. **Fig. S15:** HRMS (*m/z*): calculated (391.9886, M+H, ^{81}Br); observed (391.9880, M+1).

*4.1.3.4. Synthesis of N-(4-iodophenyl)-2-(5-phenyl-1,3,4-oxadiazol-2-ylthio) acetamide (**9d**).* Brown solid; isolated yield: 88%; R_f = 0.65 (*n*-hexane: ethyl acetate, 1:1); mp-152–156 °C. **Fig. S16:** ^{1}H NMR (400 MHz, $(CD_3)_2SO$) δ = 10.54 (s, 1H), 7.98 – 7.94 (m, 1H), 7.90 (dd, *J* = 10.3, 5.1 Hz, 1H), 7.80 (d, *J* = 7.3 Hz, 1H), 7.75 – 7.63 (m, 2H), 7.58 (ddd, *J* = 12.4, 11.5, 6.9 Hz, 2H), 7.51 – 7.37 (m, 2H), 4.35 (s, 2H). **Fig. S17:** ^{13}C NMR (150 MHz, $(CD_3)_2SO$) δ = 165.1, 165.1, 163.3, 138.4, 137.5, 132.0, 129.4, 126.3, 122.9, 121.3, 87.2 & 36.8. **Fig. S18:** IR (KBr) cm^{-1}: 3323 (Ar-**NH**CO-), 2981 (aromatic SP^2 **C—H**), 2927 (SP^3 **C—H**), 1664 (Ar-NH-**CO**-),1599, 1527 (aromatic **C═C** bending), 1445 (SP^3 **C—H,** bending), 1198 (Ar-**O-CH$_3$**); 704. **Fig. S19:** LC-MS: 438 *m/z*. **Fig. S20:** HRMS (*m/z*): calculated (437.9768, M+H); observed (437.9761, M+1).

*4.1.3.5. Synthesis of 2-(5-(2-methoxyphenyl)-1,3,4-oxadiazol-2-ylthio)-N-phenylacetamide (**9e**).* White solid; isolated yield: 88%; R_f = 0.66 (*n*-hexane: ethyl acetate, 1:1); mp-138–143 °C. **Fig. S21:** ^{1}H NMR (400 MHz, $(CD_3)_2SO$) δ = 10.44 (s, 1H), 7.62 – 7.57 (m, 2H), 7.55 (dt, *J* = 7.7 Hz, 1.3, 1H), 7.50 (t, *J* = 7.9 Hz, 1H), 7.45 (dd, *J* = 2.5, 1.5 Hz, 1H), 7.34 (dd, *J* = 10.8, 5.1 Hz, 2H), 7.20 (ddd, *J* = 8.0, 2.6, 1.2 Hz 1H), 7.09 (t, *J* = 7.4 Hz, 1H), 4.36 (s, 2H), 3.83 (s, 3H). **Fig. S22:** ^{13}C NMR (100 MHz, $(CD_3)_2SO$) δ = 165.5, 165.3, 163.9, 160.1, 139.1, 131.2, 129.3, 124.6, 124.1, 119.6, 119.1, 118.5, 111.6, 55.9, 37.3. **Fig. S23:** IR (KBr) cm^{-1}: 3268 (Ar-**NH**CO-), 3057 (aromatic SP^2 **C—H**), 2927 (SP^3 **C—H**), 1660 (Ar-NH-**CO**-), 1601, 1547 (aromatic **C═C** bending), 1443 (SP^3 **C—H**, bending), 1176 (Ar-**O-CH$_3$**), & 704; **Fig. S24:** LC-MS: 342 *m/z*. **Fig. S25:** HRMS (*m/z*): calculated (342.0907, M+H); observed (342.0906, M+1).

*4.1.3.6. Synthesis of N-(4-fluorophenyl)-2-(5-(2-methoxyphenyl)-1,3,4-oxadiazol-2-ylthio) acetamide (**9f**).* Light grey solid; isolated yield: 89%; R_f = 0.59 (*n*-hexane: ethyl acetate, 1:1); mp-161–165 °C. **Fig. S26:** ^{1}H NMR (400 MHz, $(CD_3)_2SO$) δ = 10.50 (s, 1H), 7.64 – 7.58 (m, 2H), 7.57 – 7.47 (m, 2H), 7.46 – 7.43 (m, 1H), 7.22 – 7.18 (m, 2H), 7.16 (dd, *J* = 7.3, 5.1 Hz, 1H), 4.35 (s, 2H), 3.83 (s, 3H). **Fig. S27:** ^{13}C NMR (100 MHz, $(CD_3)_2SO$) δ = 165.5, 165.3, 163.8, 160.1, 131.2, 124.5, 121.5, 119.1, 118.5, 116.0, 115.8, 111.6, 55.9, & 37.1. **Fig. S28:** IR (KBr) cm^{-1}: 3267 (Ar-**NH**CO-), 3058 (aromatic SP^2 C—H), 2927 (SP^3 **C—H**), 1681 (Ar-NH-**CO**-), 1601, 1547 (aromatic C═C Bending), 1443 (SP^3 **C—H**, bending), 1171 (Ar-**O-CH$_3$**); 704. **Fig. S29:** LC-MS: 360 *m/z*. **Fig. S30:** HRMS (*m/z*): calculated (360.0813, M+H); observed (360.0807, M+1).

*4.1.3.7. Synthesis of N-(4-bromophenyl)-2-(5-(2-methoxyphenyl)-1,3,4-oxadiazol-2-ylthio) acetamide (**9g**).* Grey solid; isolated yield: 90%; R_f = 0.69 (*n*-hexane: ethyl acetate, 1:1); mp-144–149 °C. **Fig. S31:** ^{1}H NMR (400 MHz, $(CD_3)_2SO$) δ = 10.58 (s, 1H), 7.59 – 7.57 (m, 1H), 7.56 – 7.54 (m, 1H), 7.53 (s, 2H), 7.52 – 7.47 (m, 2H), 7.46 – 7.43 (m, 1H), 7.23 – 7.18 (m, 1H), 4.36 (s, 2H), 3.83 (s, 3H). **Fig. S32:** ^{13}C NMR (100 MHz, $(CD_3)_2SO$) δ = 165.6, 165.5, 163.8, 160.1, 138.4, 132.1, 131.2, 124.5, 121.5, 119.1, 118.5, 115.7, 111.6, 55.9, 37.2. **Fig. S33:** IR (KBr) cm^{-1}: 3266 (Ar-**NH**CO-), 3059 (aromatic SP^2 **C—H**), 2926 (SP^3 **C—H**), 1681 (Ar-NH-**CO**-), 1601, 1552 (aromatic **C═C** bending), 1443 (SP^3 **C—H,** bending), 1177 (Ar-**O-CH$_3$**), & 705. **Fig. S34:** LC-MS: 420 *m/z*. **Fig. S35:** HRMS (*m/z*): calculated (421.9992, M+H, ^{81}Br); observed (421.9980, M+1).

*4.1.3.8. Synthesis of N-(4-iodophenyl)-2-(5-(2-methoxyphenyl)-1,3,4-oxadiazol-2-ylthio) acetamide (**9h**).* Brown solid; isolated yield: 92%; R_f = 0.71 (*n*-hexane: ethyl acetate, 1:1); mp-138–142 °C. **Fig. S36:** ^{1}H NMR (400 MHz, $(CD_3)_2SO$) δ = 10.56 (s, 1H), 7.70 – 7.67 (m, 1H), 7.67 – 7.64 (m, 1H), 7.56 – 7.47 (m, 2H), 7.46 – 7.44 (m, 2H), 7.43 – 7.39 (m, 1H), 7.20 (ddd, *J* = 7.9, 2.6, 1.4 Hz, 1H), 4.35 (s, 2H), 3.83 (s, 3H). **Fig. S37:** ^{13}C NMR (150 MHz, $(CD_3)_2SO$) δ = 165.0, 165.0, 163.3, 159.6, 138.4, 137.5, 130.7, 124.0, 121.3, 118.6, 118.0, 111.1, 87.2, 55.4 & 36.8. **Fig. S38:** IR (KBr) cm^{-1}: 3318 (Ar-**NH**CO-), 2925 (SP^3 **C—H**), 1662 (Ar-NH-**CO**-), 1590, 1557 (aromatic **C═C** bending), 1466 (SP^3 **C—H,** bending), 1178 (Ar-**O-CH$_3$**); & 722. **Fig. S39:** LC-MS: 468 *m/z*. **Fig. S40:** HRMS (*m/z*): calculated (467.9873, M+H); observed (467.9857, M+1).

*4.1.3.9. Synthesis of 2-(5-(3-methoxyphenyl)-1,3,4-oxadiazol-2-ylthio)-N-phenyl acetamide (**9i**).* Off-white solid; isolated yield: 92%; R_f = 0.64 (*n*-hexane: ethyl acetate, 1:1); mp-175–180 °C. **Fig. S41:** ^{1}H NMR (400 MHz, $(CD_3)_2SO$) δ = 10.43 (s, 1H), 7.93 – 7.90 (m, 1H), 7.90 – 7.87 (m, 1H), 7.60 (s, 1H), 7.58 (s, 1H), 7.34 (dd, *J* = 10.8, 5.0 Hz, 2H), 7.15 – 7.12 (m, 1H), 7.12 – 7.06 (m, 2H), 4.33 (s, 2H), 3.85 (s, 3H). **Fig. S42:** ^{13}C NMR (100 MHz, $(CD_3)_2SO$) δ = 165.5, 165.4, 163.0, 162.5, 139.1, 129.3, 128.7, 124.1, 119.6, 115.7, 115.3, 56.0, & 37.2. **Fig. S43:** IR (KBr) cm^{-1}: 3307 (Ar-**NH**CO-), 2927 (SP^3 **C—H**), 1682 (Ar-NH-**CO**-),1611, 1534 (aromatic **C═C** bending), 1473 (SP^3 **C—H,** bending), 1172 (Ar-**O-CH$_3$**); & 704. **Fig. S44:** LC-MS: 342 *m/z*. **Fig. S45:** HRMS (*m/z*): calculated (342.0907, M+H); observed (342.0901, M+1).

*4.1.3.10. Synthesis of N-(4-fluorophenyl)-2-(5-(3-methoxyphenyl)-1,3,4-oxadiazol-2-ylthio) acetamide (**9j**).* Light yellow solid; isolated yield: 90%; R_f = 0.59 (*n*-hexane: ethyl acetate, 1:1). mp-182–186 °C. **Fig. S46:** ^{1}H NMR (400 MHz, $(CD_3)_2SO$) δ = 10.50 (s, 1H), 7.92 – 7.90 (m, 1H), 7.90 – 7.88 (m, 1H), 7.64 – 7.57 (m, 2H), 7.21 – 7.14 (m, 2H), 7.13 (d, *J* = 2.0 Hz, 1H), 7.13 – 7.10 (m, 1H), 4.32 (s, 2H), 3.85 (s, 3H). **Fig. S47:** ^{13}C NMR (100 MHz, $(CD_3)_2SO$) δ = 165.5, 165.3, 162.96, 162.5, 128.7, 121.5, 121.4, 116.0, 115.8, 115.3, 56.0, & 37.1. **Fig. S48:** IR (KBr) cm^{-1}: 3315 (Ar-**NH**CO-), 3043 (aromatic SP^2 **C—H**), 2930 (SP^3 **C—H**), 1677 (Ar-NH-**CO**-),1612, 1541 (aromatic **C═C** bending), 1476 (SP^3 **C—H,** bending), 1174 (Ar-**O-CH$_3$**), & 700. **Fig. S49:** LC-MS: 360 *m/z*. **Fig. S50:** HRMS (*m/z*): calculated (360.0813, M+H); observed (360.0825, M+1).

*4.1.3.11. Synthesis of N-(4-bromophenyl)-2-(5-(3-methoxyphenyl)-1,3,4-oxadiazol-2-ylthio) acetamide (**9k**).* Light grey solid; isolated yield: 93%; R_f = 0.61 (*n*-hexane: ethyl acetate, 1:1); mp-170–175 °C. **Fig. S51:** ^{1}H NMR (400 MHz, $(CD_3)_2SO$) δ = 10.58 (s, 1H), 7.92 – 7.89 (m, 1H), 7.89 – 7.87 (m, 1H), 7.60 – 7.55 (m, 2H), 7.54 – 7.50 (m, 2H), 7.14 – 7.12 (m, 1H), 7.12 – 7.10 (m, 1H), 4.33 (s, 2H), 3.85 (s, 3H). **Fig. S52:** ^{13}C NMR (100 MHz, $(CD_3)_2SO$) δ = 165.6, 165.6, 162.9, 162.5, 138.4, 132.1, 128.7, 121.5, 115.7, 115.3, 56.0, & 37.2. **Fig. S53:** IR (KBr) cm^{-1}: 3253.0 (Ar-**NH**CO-), 2927.8 (SP^3 **C—H**), 1676.9 (Ar-NH-**CO**-), 1610.0, 1544.1 (aromatic **C═C** bending), 1442.3 (SP^3 **C—H,** bending), 1174.2 (Ar-**O-CH$_3$**), & 700.0. **Fig. S54:** LC-MS: 422 *m/z*. **Fig. S55:** HRMS (*m/z*): calculated (421.9992, M+H, ^{81}Br); observed (422.0010, M+1).

*4.1.3.12. Synthesis of N-(4-iodophenyl)-2-(5-(3-methoxyphenyl)-1,3,4-oxadiazol-2-ylthio) acetamide (**9l**).* Brown solid; isolated yield: 94%; R_f = 0.64 (*n*-hexane: ethyl acetate, 1:1); mp-172–176 °C. **Fig. S56:** ^{1}H NMR (400 MHz, $(CD_3)_2SO$) δ = 10.55 (s, 1H), 7.91 – 7.89 (m, 1H), 7.89 – 7.86 (m, 1H), 7.70 – 7.67 (m, 1H), 7.67 – 7.65 (m, 1H), 7.46 – 7.43 (m, 1H), 7.43 – 7.40 (m, 1H), 7.14 – 7.12 (m, 1H), 7.12 – 7.09 (m, 1H), 4.32 (s, 2H), 3.86 (s, 3H). **Fig. S57:** ^{13}C NMR (100 MHz, $(CD_3)_2SO$) δ = 165.6, 165.6, 162.9, 162.5, 138.9, 138.0, 128.7, 121.8, 115.7, 115.3, 56.0, & 37.2. **Fig. S58:** IR (KBr) cm^{-1}: 3250 (Ar-**NH**CO-), 2928 (SP^3 **C—H**), 1677 (Ar-NH-**CO**-), 1611, 1539 (aromatic **C═C** bending), 1442 (SP^3 **C—H,** bending), 1174 (Ar-**O-CH$_3$**), & 700. **Fig. S59:** LC-MS: 468 *m/z*. **Fig. S60:** HRMS (*m/z*): calculated (467.9873, M+H); observed (467.9895, M+1).

4.2. Biology methodology

4.2.1. Tyrosinase activity and kinetic analysis

The anti-tyrosinase activity was performed exactly same as our lab published protocol.[6] In this experiment the kojic acid was used as a standard to compare the results.[35] GraphPad Prism 5.0 was used for the analysis of IC_{50}. All experiments were repeated in triplicate. The % inhibition was calculated same as already published equation.[33] For the analysis of kinetic the different concentrations were used for the substrate and inhibitor (L-DOPA = 0.125–2 mM, inhibitor **9e** = 0.00, 0.0017, 0.0033 and 0.0066 μM). The inhibition type of ligand against tyrosinase was analysed by a Lineweaver–Burk plots (1/V). The K_i was determined from the secondary plot of 1/V against concentrations inhibitor. Other all method was followed according to our published protocol.[36]

4.2.2. Cell culture and treatment of compounds (9e, 9f, 9h, 9i & 9j)

B16F10 cells were obtained from the Korean Cell Line Bank (Seoul, Korea**)**. Cells were cultured at 37 °C under 5% CO_2 in DMEM (Sigma, St. Louis, MO, USA), supplemented with 10% fetal calf serum (FBS, WELGENE, Korea) and 50 unit/mL penicillin (Sigma) and 50 μg/mL streptomycin (Sigma). The media was changed every 2 days. Also, the most potent target compounds (**9e, 9f, 9h, 9i** & **9j**) dissolved in dimethyl sulfoxide (DMSO) and further diluted to final concentrations (0, 1, 5, 10, 20, 30, 40, 50 μg/mL). The control groups were administrated with the same amount of DMSO.

4.2.3. Melanin contents assay

B16F10 cells (3.5×10^4) were cultured in 35 mm dishes at 37 °C in an atmosphere of 5% CO_2 for 24 h. After 24 h, cells were harvested and solubilized in 1 mL of 1 M NaOH containing 10% DMSO for 2 h at 80 °C. After 2 h, cells were centrifuged at 12,000*g* for 10 min at room temperature and transfer supernatants to 96 well plate. The absorbance of the supernatants is measured at 470 nm (Molecular Devices, Sunnyvale, CA, USA).

4.2.4. Western blot analysis

Cells were washed three times with cold- phosphate buffered saline (PBS). Cells were harvested and lysed in ice-cold RIPA lysis buffer containing 50 mM Tris-HCl, pH 7.4, 150 mM sodium chloride (NaCl), 1% Nonidet P-40, and 0.1% sodium dodecyl sulfate (SDS) supplemented with phosphatase inhibitor and protease inhibitor for 30 min, followed by centrifugation at 12,000 × g for 10 min at 4 °C. Cell lysates were collected, and protein concentrations were determined using the BCA Protein assay kit (Thermo Fisher Scientific, Waltham, USA). Equivalent quantities of protein were loaded on a 9% polyacrylamide gel for electrophoresis and subsequently transferred onto 0.22 μm nitrocellulose membranes (GE Healthcare, MA, USA). The membranes were blocked with 5% non-fat dried milk dissolved in Tris-buffered saline containing 0.01% Tween-20 (TBST) for 1 hr at room temperature. The blot was then probed with the following primary antibodies: tyrosinase (1:1000) and GADPH (1:2000) antibodies at 37 °C for 4 h. After washing three times with TBST, the membranes were incubated with horseradish peroxidase-conjugated secondary antibody (1:1000) for 2 h at room temperature, and the bound antibody was visualized using an enhanced chemiluminescence solution (Jubiotech, Daejeon, Korea).

4.2.5. Cell viability assay

The cell viability was assessed by the 3-(4,5-dimethylthiazol-2-yl)-2,5-diphenyltetrazolium bromide (MTT) assay. Cells (0.5×10^5 cells/well in 96-well plates) were incubated at 37° C for 24 h and then MTT was added with a final concentration of 0.5 mg/mL per well for another 4 h. The reaction product formazan was dissolved in 10% Sodium dodecyl sulfate (SDS) with 0.01 N HCl. The cell viability was determined by reading the absorbance at 595 nm by a spectrophotometer (Bio-Rad, iMark, USA). Results are presented as the mean of three measurements ± standard deviation (n = 3).

4.2.6. Statistical analysis

Values are presented as a mean of three different experiments ± standard deviation (SD). Differences between the calculated means of each individual group were determined by one-way ANOVA. Any difference was considered statistically significant at $P < 0.05$ and $P < 0.001$.

4.3. In-silico methodology

4.3.1. Repossession of mushroom tyrosinase structure from PDB

The crystal structure of mushroom tyrosinase (Agaricus bisporus) having PDBID: 2Y9X was accessed form the Protein Data Bank (PDB) (http://www.rcsb.org).[2,6] The retrieved protein structure was minimized by using conjugate gradient algorithm and amber force field in UCSF Chimera 1.10.1.[37] The stereo-chemical properties, Ramachandran graph and values[38] of mushroom tyrosinase were assessed by Molprobity server,[39] while the Ramachandran graph was generated by Discovery Studio 2.1 Client.[40] The protein architecture and statistical percentage values of helices, beta-sheets, coils, and turns were accessed by VADAR 1.8.[41]

4.3.2. In-silico designing of synthesized compounds and molecular docking

The synthesized ligands **9(a-l)** were sketched in ACD/ChemSketch tool and access in mol format. Furthermore, UCSF Chimera 1.10.1 tool was employed to energy minimization of each ligand separately having default parameters such as steepest descent steps 100 with step size 0.02 (Å), conjugate gradient steps 100 with step size 0.02 (Å) and update interval was fixed at 10. Finally, Gasteiger charges were added using Dock Prep in ligand structure to obtain the good structure conformation. Molecular docking experiment was employed on all the synthesized ligands **9(a-l)** against α-glucosidase by using PyRx virtual screening tool with AutoDock VINA Wizard approach.[42] The grid box centre values were adjusted as for X = -2.4528, Y = 21.4728 and Z = -31.9954), respectively. We have adjusted sufficient grid box size big enough on biding pocket residues to allow the ligand to move freely in the search space. The default exhaustiveness value = 8, was adjusted in both docking to maximize the binding conformational analysis. In all docked complexes, the ligands conformational poses were keenly observed to obtain the best docking results. The docked complexes were evaluated on lowest binding energy (Kcal/mol) values and structure activity relationship analyses. The graphical depictions of all the docking complexes were carried out using Discovery Studio (2.1.0).

4.3.3. Molecular dynamic simulations (MDS)

To understand the residual backbone flexibility of protein structure, MD simulations experiment was carried out by Groningen Machine for Chemicals Simulations[43] with GROMOS 96 force field.[44] The overall system charge was neutralized by adding ions. The steepest descent approach (1000 ps) for protein structure was applied for energy minimization. For energy minimization the nsteps = 50,000 were adjusted with energy step size (emstep) 0.01 value. Particle Mesh Ewald (PME)

method was employed for energy calculation and for electrostatic and van der waals interactions; cut-off distance for the short-range VdW (rvdw) was set to 14 Å, whereas neighbour list (rlist) and nstlist values were adjusted as 1.0 and 10, respectively, in em.mdp file.[45] It permits the use of the Ewald summation at a computational cost comparable with that of a simple truncation method of 10 Å or less, and the linear constraint solver (LINCS).[46] Algorithm was used for covalent bond constraints and the time step was set to 0.002 ps. Finally, the molecular dynamics simulation was carried out at 1000 ps in md.mdp file. Different structural evaluations such as root mean square deviations and fluctuations (RMSD/RMSF), solvent accessible surface areas (SASA) and radii of gyration (Rg) of back bone residues were analysed through Xmgrace software (http://plasma-gate.weizmann.ac.il/Grace/) and UCSF Chimera 1.10.1 software.

4.3.4. Molecular dynamic simulation analysis

Based on *in-vitro* and docking results, **9e** docked complex was selected for dynamic simulation analysis using GROMACS 5.1 tool. The protein backbone structural fluctuated behaviour of **9e** docking complex was examined by generating RMSD/F, R_g and SASA graphs.

Declaration of Competing Interest

The authors declare that they have no known competing financial interests or personal relationships that could have appeared to influence the work reported in this paper.

Acknowledgement

This research was supported by Basic Science Research Program through the National Research Foundation of Korea (NRF) funded by the Ministry of Education (NRF- 2019R1I1A3A01059089).

Appendix A. Supplementary material

Supplementary data to this article can be found online at https://doi.org/10.1016/j.bmc.2021.116222.

References

1 Zhao Z, Liu G, Meng Y, et al. Synthesis and anti-tyrosinase mechanism of the substituted vanillyl cinnamate analogues. *Bioorg Chem*. 2019;93, 103316. https://doi.org/10.1016/j.bioorg.2019.103316.
2 Vanjare BD, Mahajan PG, Dige NC, et al. Novel 1,2,4-triazole analogues as mushroom tyrosinase inhibitors: synthesis, kinetic mechanism, cytotoxicity and computational studies. *Mol Divers*. 2020. https://doi.org/10.1007/s11030-020-10102-5.
3 Roulier B, Pérès B, Haudecoeur R. Advances in the Design of Genuine Human Tyrosinase Inhibitors for Targeting Melanogenesis and Related Pigmentations. *J Med Chem*. 2020;63(22):13428–13443. https://doi.org/10.1021/acs.jmedchem.0c00994.
4 Abbas Q, Ashraf Z, Hassan M, et al. Development of highly potent melanogenesis inhibitor by in vitro, in vivo and computational studies. *Drug Des Devel Ther*. 2017;11: 2029–2046. https://doi.org/10.2147/DDDT.S137550.
5 Bang EJ, Noh SG, Ha S, et al. Evaluation of the novel synthetic tyrosinase inhibitor (z)-3-(3-bromo-4-hydroxybenzylidene) thiochroman-4-one (MHY1498) In vitro and in silico. *Molecules*. 2018;23:1–11. https://doi.org/10.3390/molecules23123307.
6 Dige NC, Mahajan PG, Raza H, et al. Ultrasound mediated efficient synthesis of new 4-oxoquinazolin-3(4H)-yl)furan-2-carboxamides as potent tyrosinase inhibitors: Mechanistic approach through chemoinformatics and molecular docking studies. *Bioorg Chem*. 2019;92, 103201. https://doi.org/10.1016/j.bioorg.2019.103201.
7 Maertens JA. History of the development of azole derivatives. *Clin Microbiol Infect*. 2004;10:1–10. https://doi.org/10.1111/j.1470-9465.2004.00841.x.
8 De B, Adhikari I, Nandy A, Saha A, Goswami BB. In silico modelling of azole derivatives with tyrosinase inhibition ability: Application of the models for activity prediction of new compounds. *Comput Biol Chem*. 2018;74:105–114. https://doi.org/10.1016/j.compbiolchem.2018.03.007.
9 Zolghadri S, Bahrami A, Hassan Khan MT, et al. A comprehensive review on tyrosinase inhibitors. *J Enzyme Inhib Med Chem*. 2019;34:279–309. https://doi.org/10.1080/14756366.2018.1545767.
10 Khan MTH. Heterocyclic Compounds Against the Enzyme Tyrosinase Essential for Melanin Production: Biochemical Features of Inhibition. *Bioactive Heterocycles III*. 2007. https://doi.org/10.1007/7081_2007_077.
11 De Oliveira CS, Lira BF, Barbosa-Filho JM, Lorenzo JGF, De Athayde-Filho PF. Synthetic Approaches and Pharmacological Activity of 1,3,4-Oxadiazoles: A Review of the Literature from 2000-2012. Molecules 2012;17. http://dx.doi.10.3390/molecules170910192.
12 Mutchu BR, Kotra V, Onteddu SR, Boddapati SNM, Bollikolla HB. Synthesis, Cytotoxicity and Antimicrobial Evaluation of Some New 2-Aryl,5-Substituted 1,3,4-Oxadiazoles and 1,3,4-Thiadiazoles. *Chem Africa*. 2019;2:15–20. https://doi.org/10.1007/s42250-018-00034-x.
13 Aziz H, Mahmood A, Zaib S, et al. Synthesis, characterization, alkaline phosphatase inhibition assay and molecular modeling studies of 1-benzylidene-2-(4-tert-butylthiazol-2-yl) hydrazines. *J Biomol Struct Dyn*. 2020. https://doi.org/10.1080/07391102.2020.1802336.
14 Aziz H, Mahmood A, Zaib S, et al. Synthesis, characterization, in vitro tissue-nonspecific alkaline phosphatase (TNAP) and intestinal alkaline phosphatase (IAP) inhibition studies and computational evaluation of novel thiazole derivatives. *Bioorg Chem*. 2020;102, 104088. https://doi.org/10.1016/j.bioorg.2020.104088.
15 Jha KK, Samad A, Kumar Y, et al. Design, synthesis and biological evaluation of 1,3,4-oxadiazole derivatives. *Eur J Med Chem*. 2010;45:4963–4967. https://doi.org/10.1016/j.ejmech.2010.08.003.
16 Palit R, Saraswat N, Sahoo J. Review on Substituted 1,3,4-Oxadiazole and Its Biological Activities. *Int Res J Pharm*. 2016;7:1–7. https://doi.org/10.7897/2230-8407.07212.
17 Bala S, Kamboj S, Kajal A, Saini V, Prasad DN. 1,3,4-Oxadiazole Derivatives: Synthesis, Characterization, Antimicrobial Potential, and Computational Studies. *Biomed Res Int*. 2014;2014. https://doi.org/10.1155/2014/172791.
18 Bondock S, Adel S, Etman HA, Badria FA. Synthesis and antitumor evaluation of some new 1,3,4-oxadiazole-based heterocycles. *Eur J Med Chem*. 2012;48:192–199. https://doi.org/10.1016/j.ejmech.2011.12.013.
19 Paruch K, Popiołek Ł, Wujec M. Antimicrobial and antiprotozoal activity of 3-acetyl-2,5-disubstituted-1,3,4-oxadiazolines: a review. *Med Chem Res*. 2020;29:1–16. https://doi.org/10.1007/s00044-019-02463-w.
20 Lam KW, Syahida A, Ul-Haq Z, Rahman MBA, Lajis NH. Synthesis and biological activity of oxadiazole and triazolothiadiazole derivatives as tyrosinase inhibitors. *Bioorg Med Chem Lett*. 2010;20:3755–3759. https://doi.org/10.1016/j.bmcl.2010.04.067.
21 Bandgar BP, Adsul LK, Chavan HV, et al. Synthesis, biological evaluation, and molecular docking of N-{3-[3-(9-methyl-9H-carbazol-3-yl)-acryloyl]-phenyl}-benzamide/amide derivatives as xanthine oxidase and tyrosinase inhibitors. *Bioorg Med Chem*. 2012;20:5649–5657. https://doi.org/10.1016/j.bmc.2012.07.001.
22 D'Mello SAN, Finlay GJ, Baguley BC, Askarian-Amiri ME. Signaling pathways in melanogenesis. *Int J Mol Sci*. 2016;17:1–18. https://doi.org/10.3390/ijms17071144.
23 Lin LC, Chen CY, Kuo CH, et al. 36H: A Novel Potent Inhibitor for Antimelanogenesis. *Oxid Med Cell Longev*. 2018; 2018.. https://doi.org/10.1155/2018/6354972.
24 Ullah S, Kang D, Lee S, et al. Synthesis of cinnamic amide derivatives and their anti-melanogenic effect in α-MSH-stimulated B16F10 melanoma cells. *Eur J Med Chem*. 2019;161:78–92. https://doi.org/10.1016/j.ejmech.2018.10.025.
25 Yu JS, Kim AK. Effect of combination of taurine and azelaic acid on antimelanogenesis in murine melanoma cells. *J Biomed Sci*. 2010;17:8–11. https://doi.org/10.1186/1423-0127-17-S1-S45.
26 Saeedi M, Eslamifar M, Khezri K. Kojic acid applications in cosmetic and pharmaceutical preparations. *Biomed Pharmacother*. 2019;110:582–593. https://doi.org/10.1016/j.biopha.2018.12.006.
27 Ashraf Z, Rafiq M, Nadeem H, et al. Carvacrol derivatives as mushroom tyrosinase inhibitors; synthesis, kinetics mechanism and molecular docking studies. *PLoS ONE*. 2017;12:1–17. https://doi.org/10.1371/journal.pone.0178069.
28 Hassan M, Ashraf Z, Abbas Q, Raza H, Seo SY. Exploration of Novel Human Tyrosinase Inhibitors by Molecular Modeling, Docking and Simulation Studies. *Interdiscip Sci Comput Life Sci*. 2018. https://doi.org/10.1007/s12539-016-0171-x.
29 Hassan M, Abbas Q, Ashraf Z, Moustafa AA, Seo SY. Pharmacoinformatics exploration of polyphenol oxidases leading to novel inhibitors by virtual screening and molecular dynamic simulation study. *Comput Biol Chem*. 2017. https://doi.org/10.1016/j.compbiolchem.2017.02.012.
30 Hassan M, Shahzadi S, Seo SY, Alashwal H, Zaki N, Moustafa AA. Molecular docking and dynamic simulation of AZD3293 and solanezumab effects against BACE1 to treat alzheimer's disease. *Front Comput Neurosci*. 2018. https://doi.org/10.3389/fncom.2018.00034.
31 Vanjare BD, Mahajan PG, Hassan M, et al. Design, Synthesis, Photophysical Properties, Biological Estimation and Molecular Docking Studies of Novel Schiff Base Derivatives as Potential Urease Inhibitors. *J Fluoresc*. 2018. https://doi.org/10.1007/s10895-018-2289-1.
32 Channar PA, Saeed A, Albericio F, et al. Sulfonamide-Linked ciprofloxacin, sulfadiazine and amantadine derivatives as a novel class of inhibitors of jack bean urease; synthesis, kinetic mechanism and molecular docking. *Molecules*. 2017. https://doi.org/10.3390/molecules22081352.
33 Larik FA, Saeed A, Channar PA, et al. Design, synthesis, kinetic mechanism and molecular docking studies of novel 1-pentanoyl-3-arylthioureas as inhibitors of mushroom tyrosinase and free radical scavengers. *Eur J Med Chem*. 2017;141: 273–281. https://doi.org/10.1016/j.ejmech.2017.09.059.
34 Vanjare BD, Mahajan PG, Dige NC, et al. Synthesis of novel xanthene based analogues: Their optical properties, jack bean urease inhibition and molecular modelling studies. *Spectrochim Acta - Part A Mol Biomol Spectrosc*. 2020;241, 118667. https://doi.org/10.1016/j.saa.2020.118667.
35 Saeed A, Mahesar PA, Channar PA, et al. Synthesis, molecular docking studies of coumarinyl-pyrazolinyl substituted thiazoles as non-competitive inhibitors of mushroom tyrosinase. *Bioorg Chem*. 2017;74:187–196. https://doi.org/10.1016/j.bioorg.2017.08.002.

36 Abbas Q, Raza H, Hassan M, Phull AR, Kim SJ, Seo SY. Acetazolamide Inhibits the Level of Tyrosinase and Melanin: An Enzyme Kinetic, In Vitro, In Vivo, and In Silico Studies. *Chem Biodivers*. 2017;14:1–13. https://doi.org/10.1002/cbdv.201700117.

37 Pettersen EF, Goddard TD, Huang CC, et al. UCSF Chimera - A visualization system for exploratory research and analysis. *J Comput Chem*. 2004. https://doi.org/10.1002/jcc.20084.

38 Lovell SC, Davis IW, Iii WBA, et al. Structure validation by Calpha geometry: Phi, psi and Cbeta deviation. *Proteins*. 2003.

39 Chen VB, Arendall WB, Headd JJ, et al. MolProbity: All-atom structure validation for macromolecular crystallography. *Acta Crystallogr Sect D Biol Crystallogr*. 2010. https://doi.org/10.1107/S0907444909042073.

40 Diego S. Discovery Studio Modeling Environment Release 2.1. Accelerys Softw Inc; 2007.

41 Willard L, Ranjan A, Zhang H, et al. VADAR: A web server for quantitative evaluation of protein structure quality. *Nucleic Acids Res*. 2003. https://doi.org/10.1093/nar/gkg565.

42 Dallakyan S, Olson AJ. Small-molecule library screening by docking with PyRx. *Methods Mol Biol*. 2015. https://doi.org/10.1007/978-1-4939-2269-7_19.

43 Pronk S, Páll S, Schulz R, et al. GROMACS 4.5: A high-throughput and highly parallel open source molecular simulation toolkit. *Bioinformatics*. 2013. https://doi.org/10.1093/bioinformatics/btt055.

44 Chiu SW, Pandit SA, Scott HL, Jakobsson E. An improved united atom force field for simulation of mixed lipid bilayers. *J Phys Chem B*. 2009. https://doi.org/10.1021/jp807056c.

45 Wang H, Dommert F, Holm C. Optimizing working parameters of the smooth particle mesh Ewald algorithm in terms of accuracy and efficiency. *J Chem Phys*. 2010. https://doi.org/10.1063/1.3446812.

46 Amiri S, Sansom MSP, Biggin PC. Molecular dynamics studies of AChBP with nicotine and carbamylcholine: The role of water in the binding pocket. *Protein Eng Des Sel*. 2007. https://doi.org/10.1093/protein/gzm029.